Supplement of

Seasonal variability, sources, and parameterization of ice-nucleating particles in the Rocky Mountain region

Ruichen Zhou, Russell Perkins, Drew Juergensen, Kevin Barry, Kelton Ayars, Oren Dutton, Paul DeMott, Sonia Kreidenweis

Department of Atmospheric Science, Colorado State University, Fort Collins, Colorado 80523, USA

Text S1. Source apportionment

The PMF analysis was performed using the EPA PMF 5.0 software and using data from the White River IMPROVE site, which is located near the SAIL campaign (~ 30 km distant), from January 2014 to April 2024 to understand the aerosol sources impacting this region. The atmospheric concentrations in the $PM_{2.5}$ fraction of nineteen elements (Al, As, Br, Ca, Cl, Cr, Cu, Fe, K, Mg, Mn, Na, Ni, Pb, Se, Si, Ti, V, and Zn), nitrate, sulfate, elemental carbon, organic carbon, and the mass concentrations of PM_{10} and coarse mass, which was calculated by subtracting $PM_{2.5}$ from PM_{10}, were used for the source apportionment. The concentrations were reported based on local conditions of temperature and pressure. The uncertainties in concentrations for various components were used directly as reported in the IMPROVE dataset. There are no uncertainties reported for organic carbon and elemental carbon before 2017. These uncertainties were therefore calculated based on the method introduced in (Niño, 2021) and the IMPROVE standard operating procedure #351 (https://vista.cira.colostate.edu/improve/wp-content/uploads/2019/06/IMPROVE-SOP-351_Data-Processing-and-Validation_06.2019.pdf). Based on the signal/noise ratio for each component, As, Cr, Ni, Pb, Se, were categorized in the "bad" category and excluded from PMF rotations. Cu and V were put into the "weak" category and their uncertainties were tripled. PM_{10} was used as a total variable to constrain the total aerosol mass concentrations. PMF was run multiple times, exploring 4–7 factor solutions.

A 5-factor solution was chosen as an optimal solution based on the Q/Q_{exp} and interpretation of the physical meanings of the factors. The factor profiles and their time series are shown in Figure S5. The five factors were identified as coarse dust, fine dust, biomass burning, sulfate-dominated, and nitrate-dominated sources. Coarse and fine dusts had high contributions from Al, Ca, Fe, Mg, and Si, which are main components of mineral dust. Coarse dust explained more than 90% of the coarse mass, while there was no contribution from coarse mass in the fine dust factor. These mineral elements contributions were higher in fine dust than in coarse dust, which is mainly due to the fact that elemental analyses of IMPROVE samples were performed only on the $PM_{2.5}$ fraction. The biomass burning factor was strongly associated with organic and elemental carbon, which are mainly from combustion processes, and K, a tracer of biomass burning. The other two factors are dominated by nitrate and sulfate, which are related to the formation of secondary aerosols and

possibly some primary emissions from regional sources that include energy production and distant urban regions.

From the 10-year time series (Figure S5b), the seasonal variation of sources was clearly identified. Dust concentrations presented a seasonal cycle with higher concentrations in spring, summer, and fall. Fine dust mostly occurred in spring seasons except in 2020, while coarse dust was prevalent in spring, summer, and fall with highest concentrations in summer. This suggests different sources for fine and coarse dust. There were significantly higher fine dust concentrations in 2022, and high coarse dust concentrations in 2022 and 2023. Biomass burning showed an event-driven time series. There were intense wildfire smoke events detected at White River in 2020 and 2021. Biomass burning in the western U.S. is an annual occurrence and contributes to aerosol loadings through summer and early fall, although the locations of the most severe fires and the dominant transport pathways vary interannually (Brey et al., 2018). The sulfate-dominated factor had higher concentrations in warm seasons, suggesting the importance of photochemical processes in driving secondary aerosol formation. The nitrate-dominated factor was highest in spring, which may relate to the combined impacts of dust and photochemistry.

PMF analyses were also performed for two additional regional IMPROVE sites, Mount Zirkel Wilderness (MOZI) and Rocky Mountain NP (ROMO), which are located approximately 150 km north and 170 km northeast of the White River site, respectively. These two sites also resolved similar 5-factor solutions. The seasonal patterns of coarse dust, fine dust, and biomass burning were highly consistent among all 3 sites (Figures S5 and S7), although with differences in attributed concentrations. This suggests that these aerosol types are largely influenced by regional sources that impact aerosol concentrations across a broad region of the Colorado Rockies. This comparison supports the assumption that aerosol types observed at the SAIL campaign site and at WHRI (30 km away) are likely similar, and that the source apportionment results can be used to estimate dominant aerosol types for the SAIL campaign.

Test S2. qPCR analysis of *Pseudomonas syringae*

To investigate potential *Pseudomonas syringae* influence, which may be indicative of snowmaking activities, DNA was extracted using the DNeasy PowerSoil Pro Kit (Qiagen) from 8 samples with an INP spectrum similar to Snomax® and 4 reference samples without that spectrum (i.e., normal winter samples) with. Half of each filter was used for extraction, and DNA was eluted into 60 µL of CD6. qPCR was performed at University of Colorado Boulder with the QuantStudio 3, using the Applied Biosystems™ PowerUp™ SYBR™ Green Master Mix, established *Pseudomonas* specific primers (Guilbaud et al., 2016), and a GBlock Gene Fragment (IDT) to make standards that ranged from 101-108 copies/µL. All reactions were performed in triplicate.

The results are shown in Figure S4. DNA from *Pseudomonas syringae* was detected in four samples, while no *Pseudomonas syringae* was found in the reference samples. This result supports the conclusion that some samples collected during winter were affected by snowmaking activities. Although *Pseudomonas syringae* was not detected in all eight samples that had an INP spectrum similar to Snomax, this possibly due to low DNA concentrations. Given that their INP concentration spectra are highly similar to that of Snomax, all eight samples are suspected to have been affected by snowmaking and were excluded from further analysis in this study.

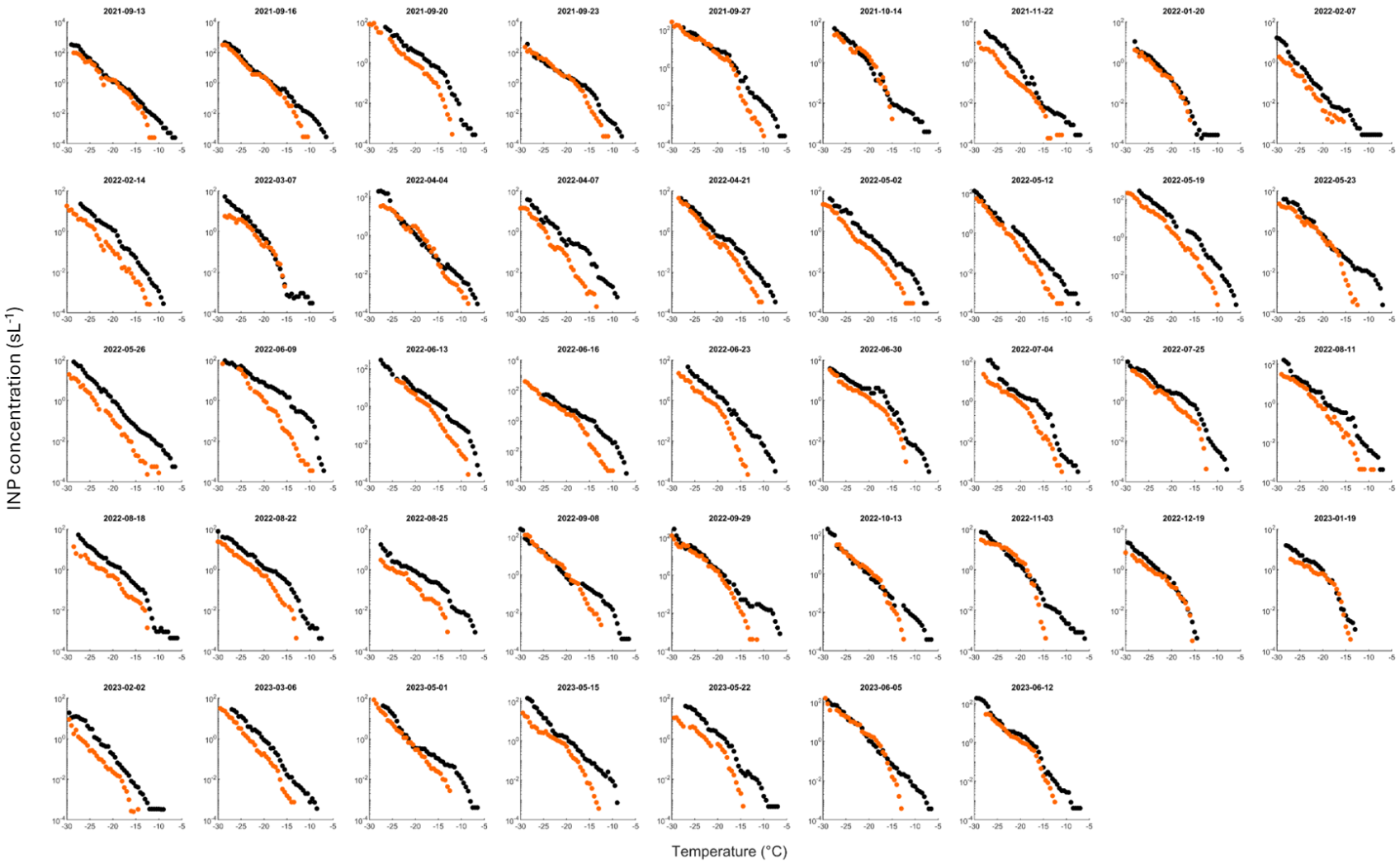

Figure S1. The INP temperature spectra of samples that were subjected to additional treatments. The base analyses (black dots) are shown along with spectra after heat treatment (orange dots). For clarity, uncertainties are not shown here.

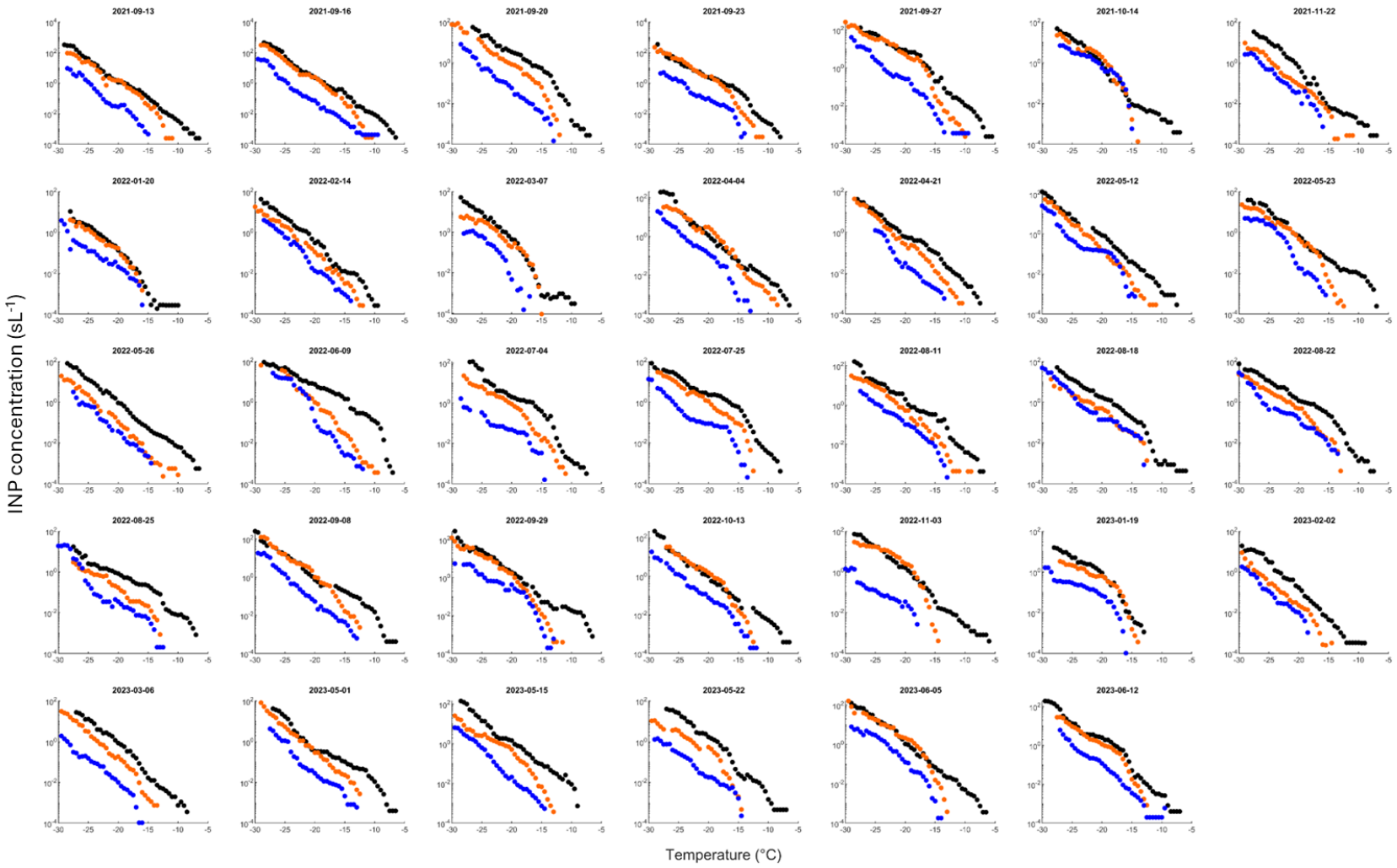

Figure S2. The INP temperature spectra of samples with base analysis (black dot), heat treatment (orange dot), and H_2O_2 treatment (blue dot). For clarity, uncertainties are not shown here.

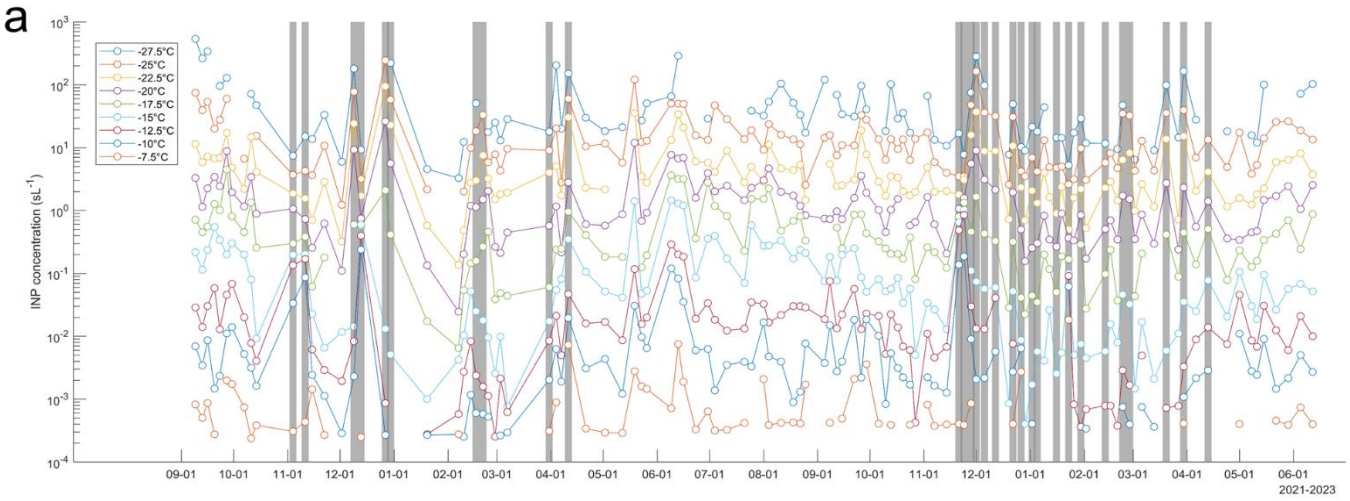

Figure S3. INP concentrations (sL^{-1}) at temperatures from −7.5 ℃ to −27.5 ℃ (interval of 2.5℃) for all analyzed samples during SAIL campaign. The grey shadows show samples collected during cloud seeding and affected by snowmaking activities.

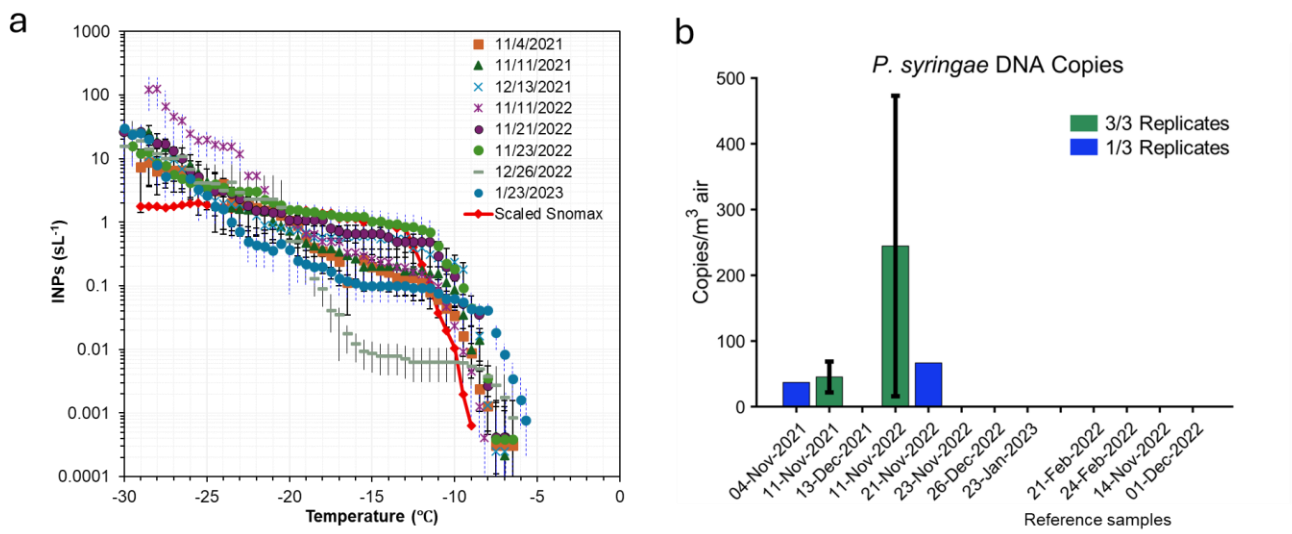

Figure S4. (a) INP temperature spectra for wintertime samples with a distinct shape similar to that of Snomax. (b) *P. syringae* DNA copy numbers in these samples and in reference samples presumed not affected by Snomax, according to inspection of their INP spectra.

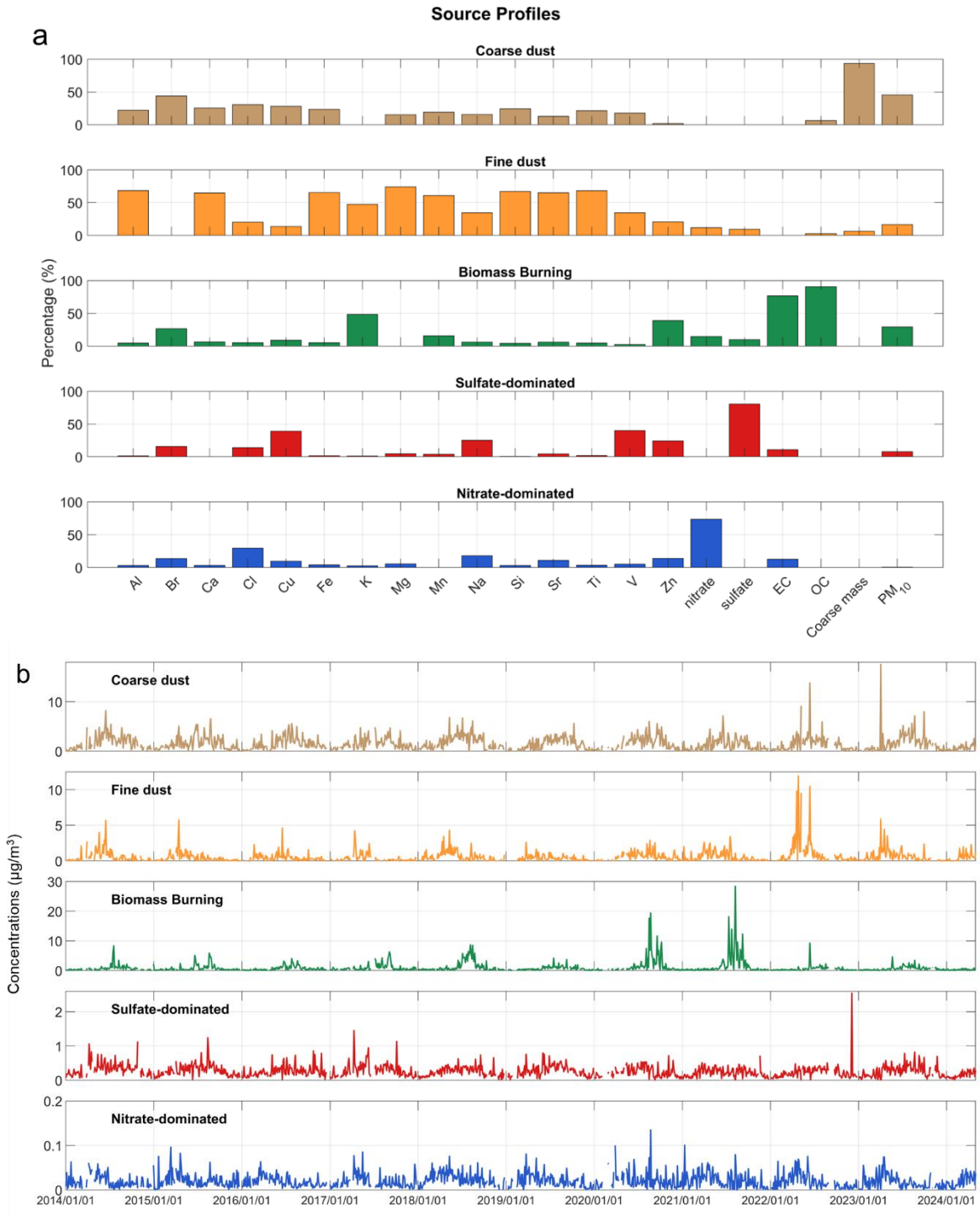

Figure S5. (a) Factor profiles and (b) time series of aerosol type concentrations (μg m^{-3}) for the five-factor solution from the PMF analysis of data from the IMPROVE site at White River.

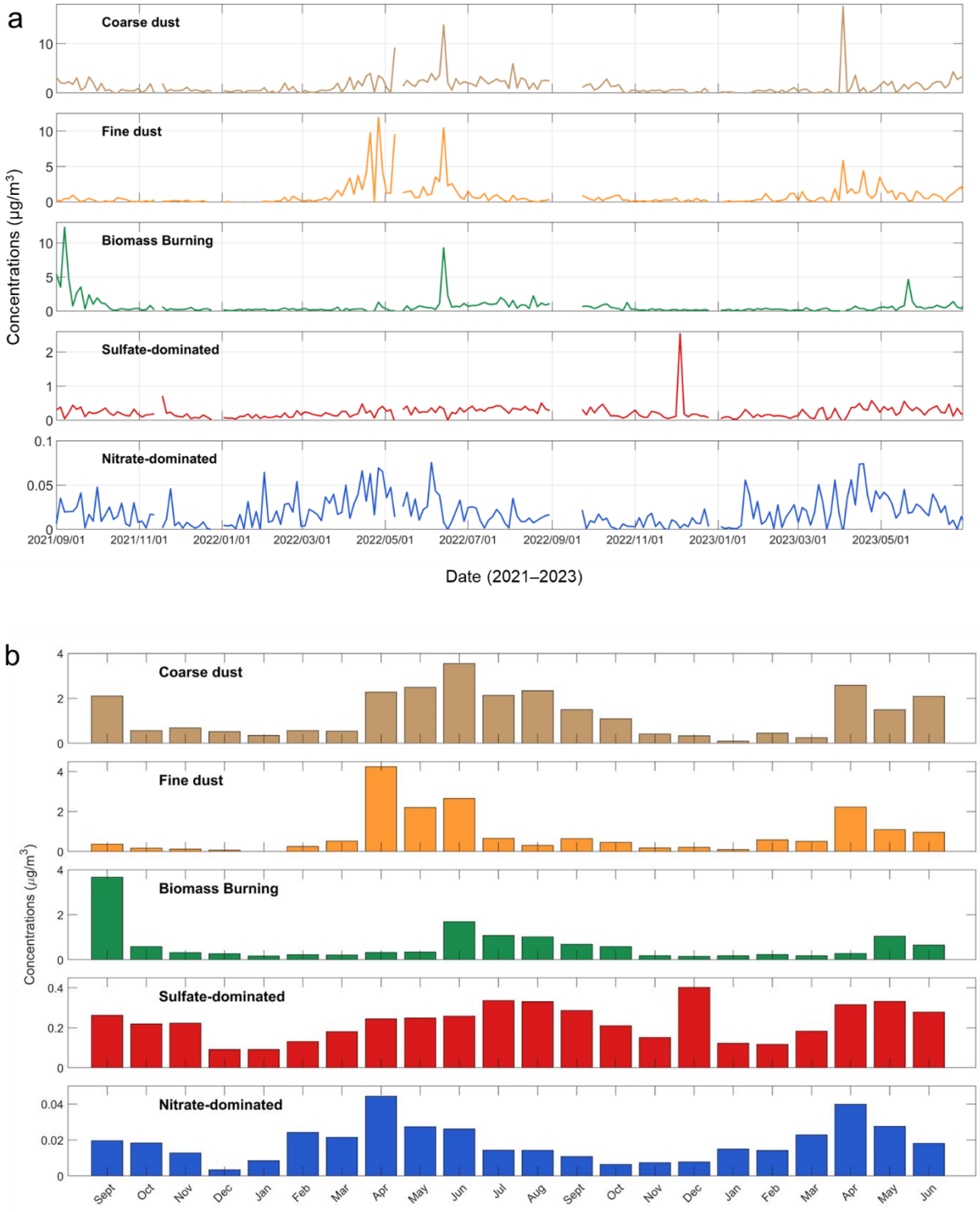

Figure S6. (a) Time series of mass concentrations (μg m^{-3}) attributed to the five factors during the period of the SAIL campaign (September 2021 to June 2023), and (b) their monthly mean concentrations.

Figure S7. Time series of aerosol type concentrations (μg m^{-3}) for the five-factor solution from the PMF analysis of data from the IMPROVE site at (a) Mount Zirkel Wilderness (MOZI) and (b) Rocky Mountain NP (ROMO).

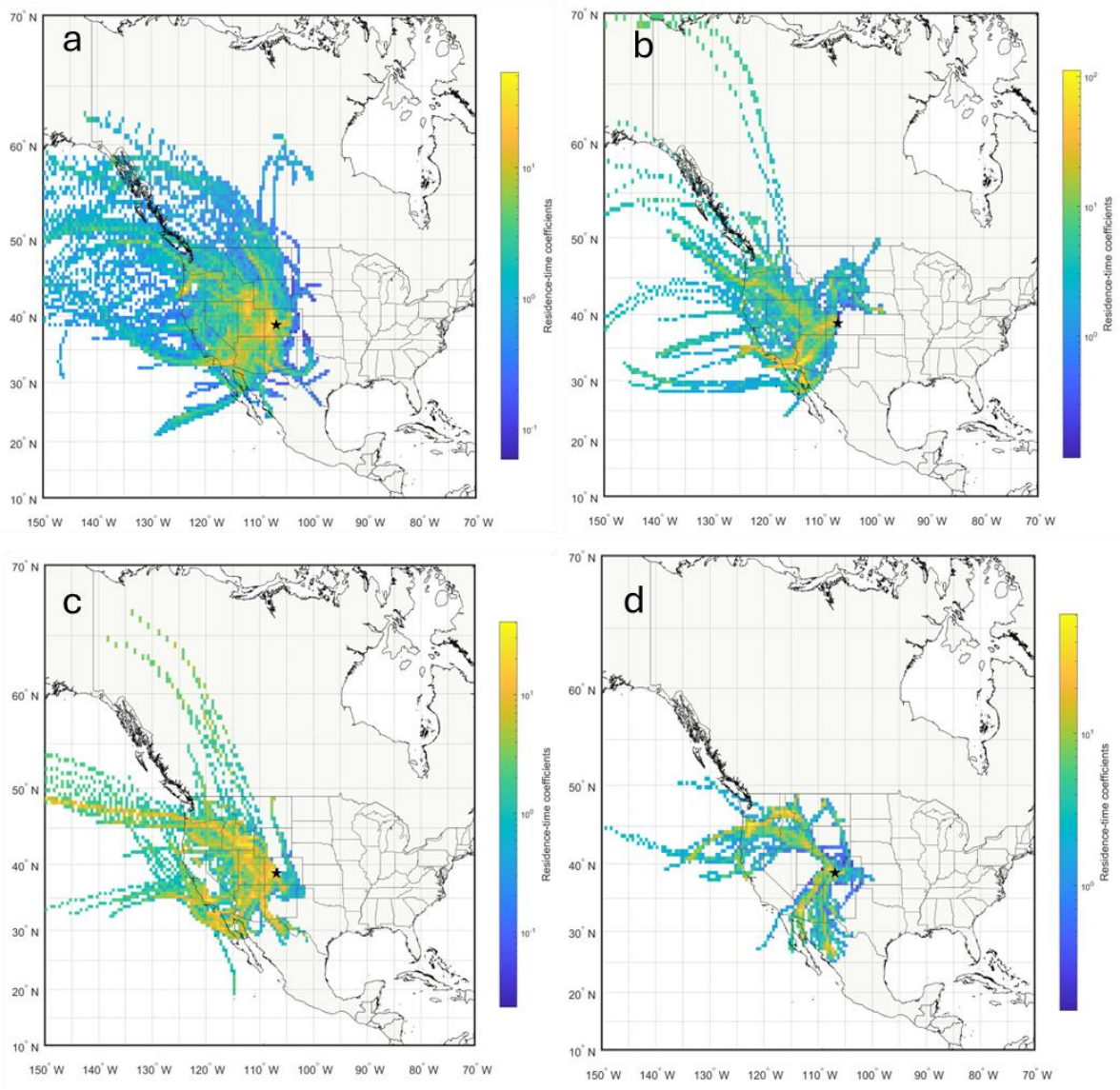

Figure S8. Residence-time weighted back trajectories for samples that were categorized as dominated by (a) coarse dust, (b) fine dust, (c) dust, and (d) biomass burning. The categorization was based on aerosol source contributions derived from the PMF analysis; details of the categorization method are provided in the Methods section.

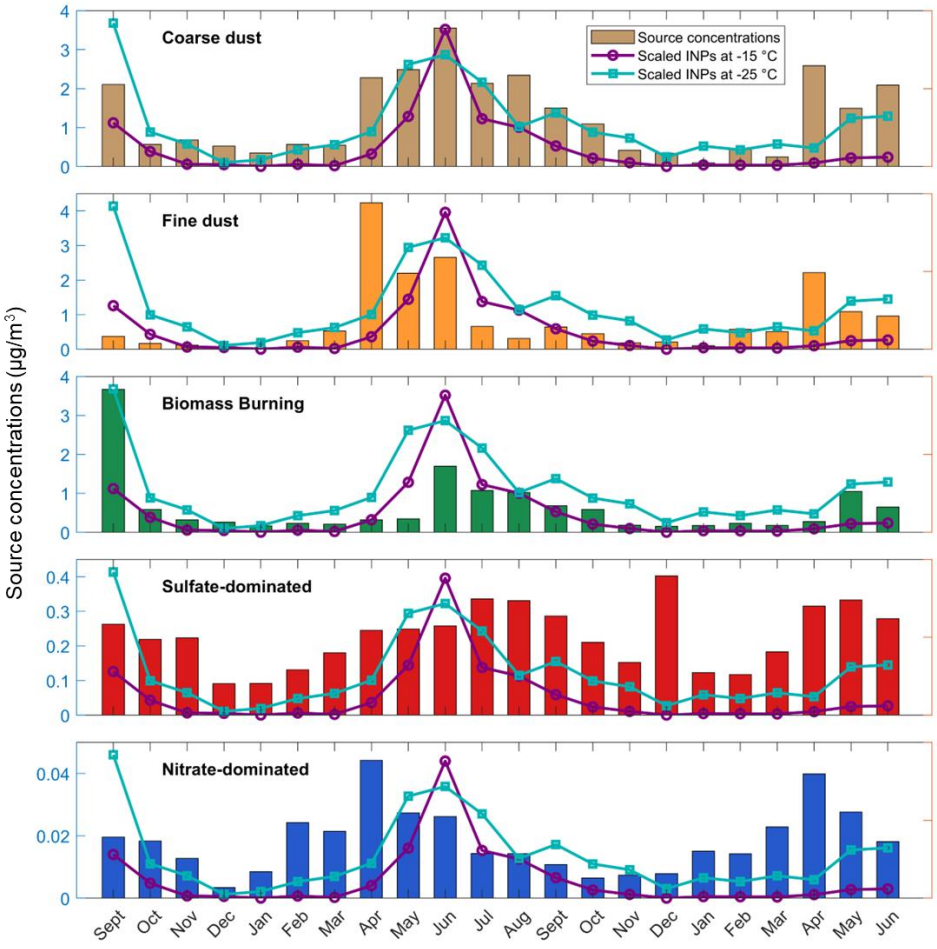

Figure S9. Monthly mean INP concentrations (lines, arbitrary scaling) at −15 ℃ and −25 ℃ and monthly mean aerosol mass concentrations (bars) from coarse dust, fine dust, biomass burning, sulfate-dominated, and nitrate-dominated sources.

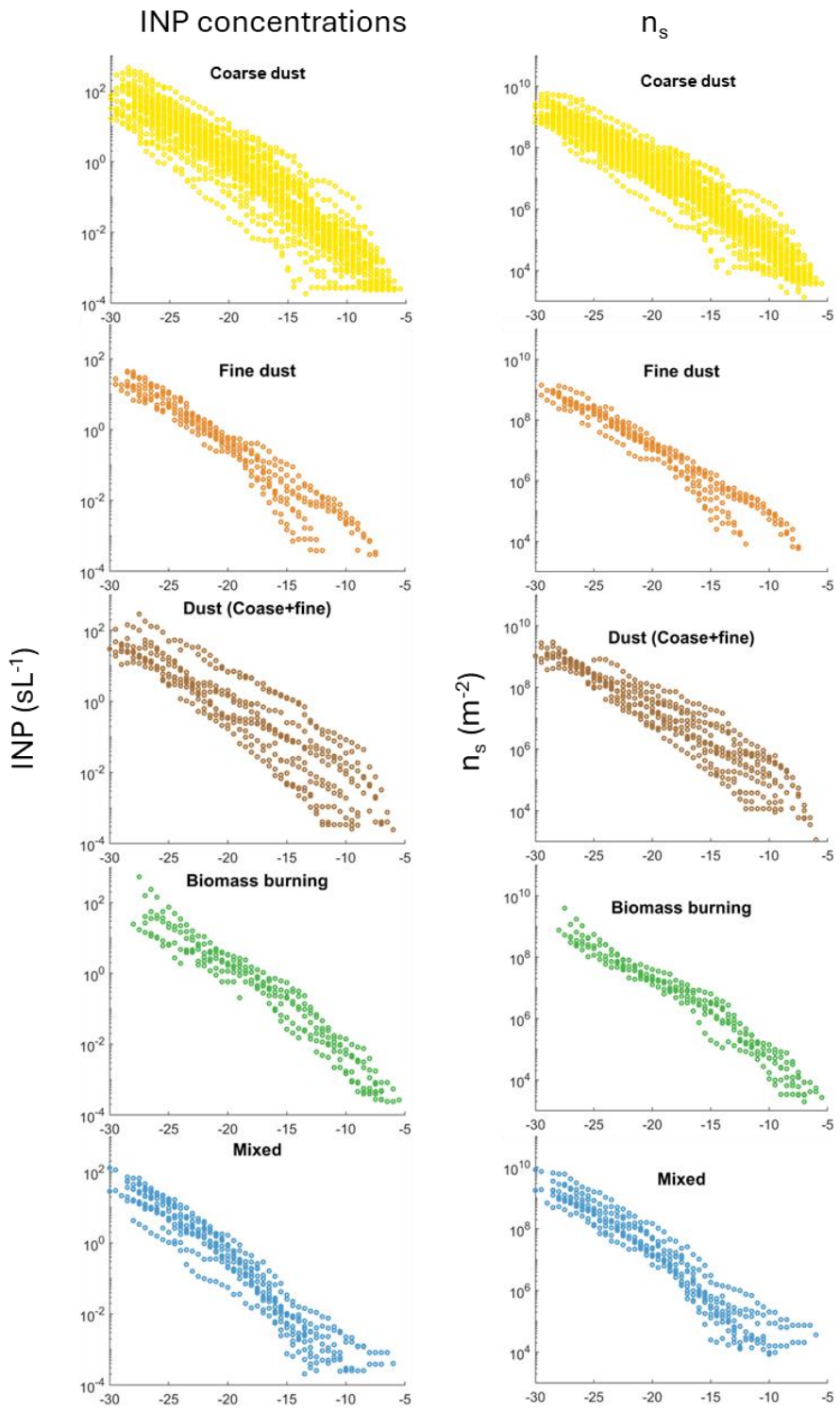

Figure S10. Total INP temperature spectra (sL^{-1}) and IN active surface site density (n_s, m^{-2}) stratified by dominant aerosol source (coarse dust, dust, fine dust, biomass burning, and mixed). n_s is calculated based on the surface area of particles larger than 500 nm.

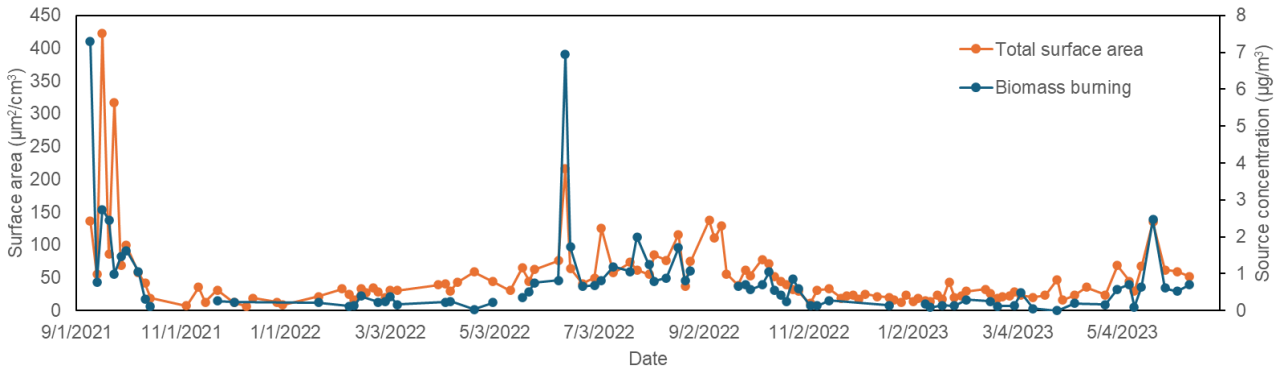

Figure S11. Relationships between biomass burning mass concentration (µg/m^3) and total surface area concentrations (µm^2/cm^3).

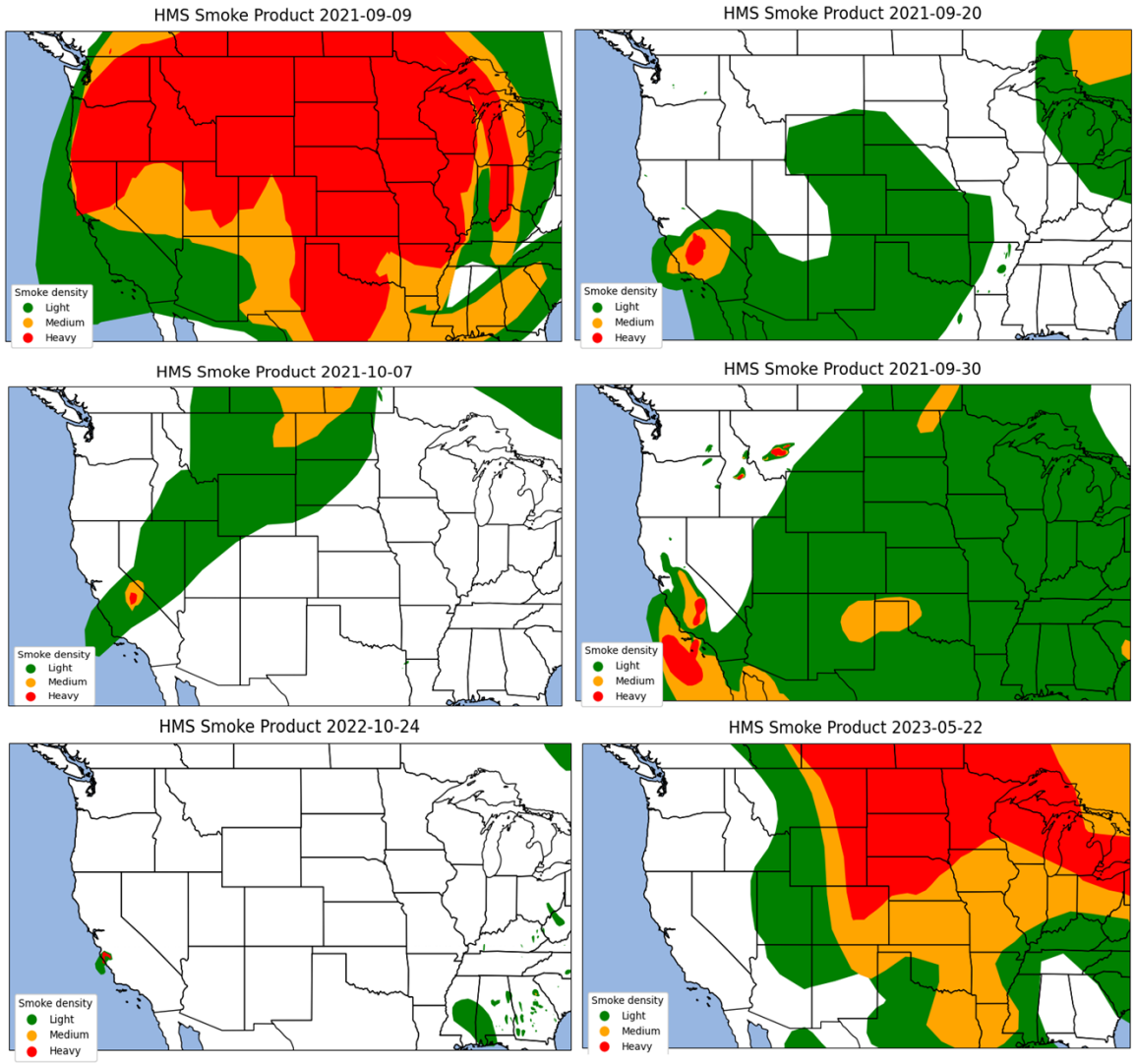

Figure S12. NOAA Hazard Mapping System products for the sample days, which are dominated by biomass burning aerosols.

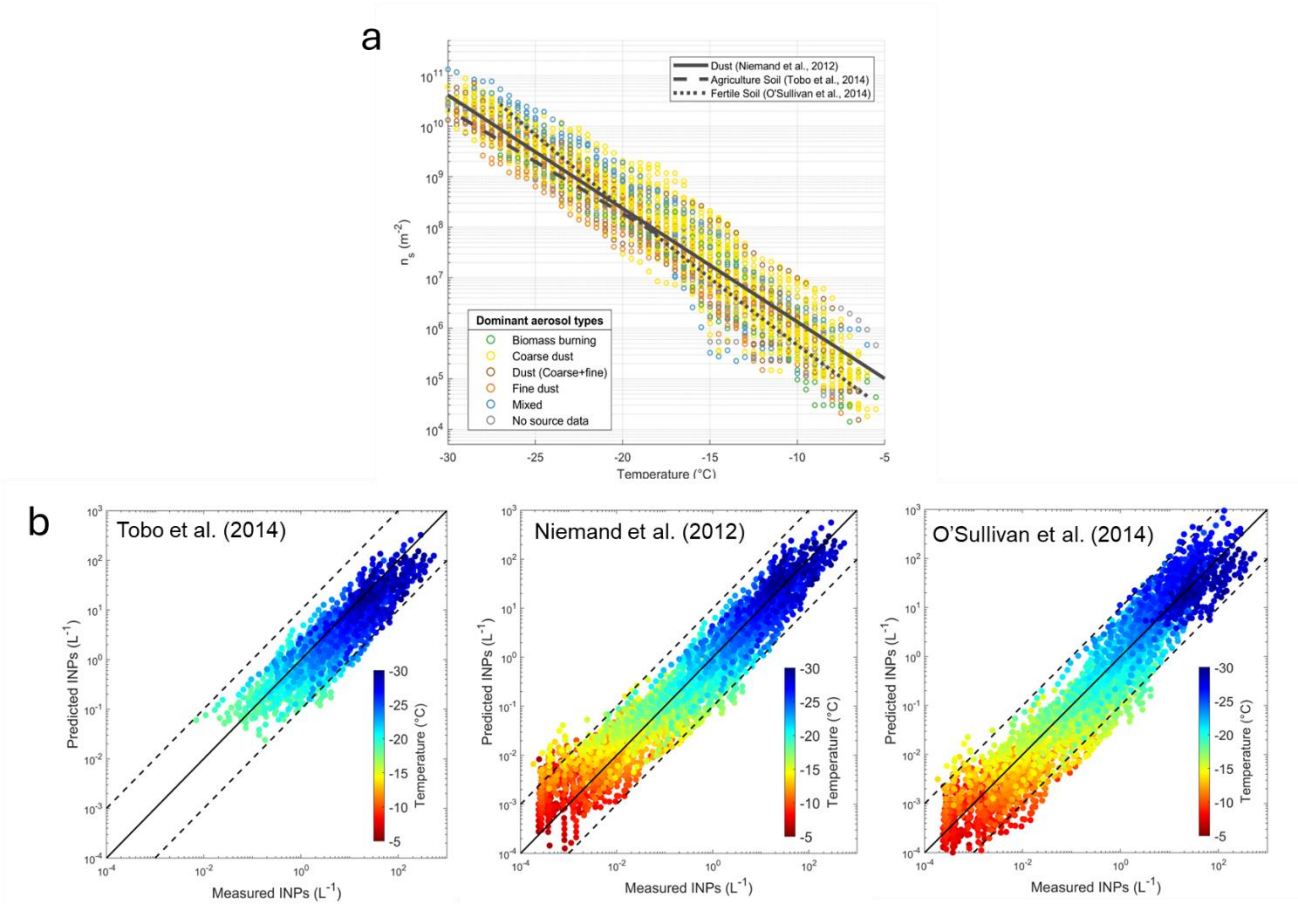

Figure S13. (a) IN active surface site density (n_s, m^{-2}) calculated based on the surface area of particles larger than 500 nm, compared with those derived from agricultural soil (Tobo et al., 2014), dust (Niemand et al., 2012), and fertile soil (O'Sullivan et al., 2014). (b) Estimated SAIL INP concentrations using parameterizations from Tobo et al. (2014), Niemand et al. (2012), and O'Sullivan et al. (2014) and surface area of particles larger than 500 nm, compared with SAIL observations.

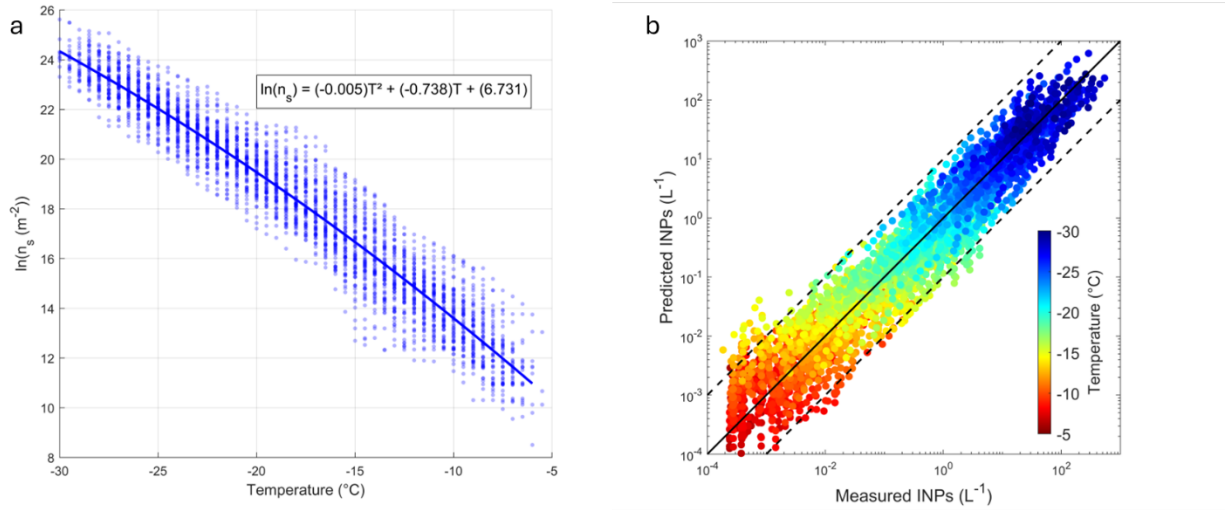

Figure S14. (a) A single polynomial parameterization for the measured n_s ln (n_s) = $-0.005T^2 - 0.738T + 6.003$ (-30 °C < T < -6 °C), and (b) predicted INP concentrations based on this parameterization.

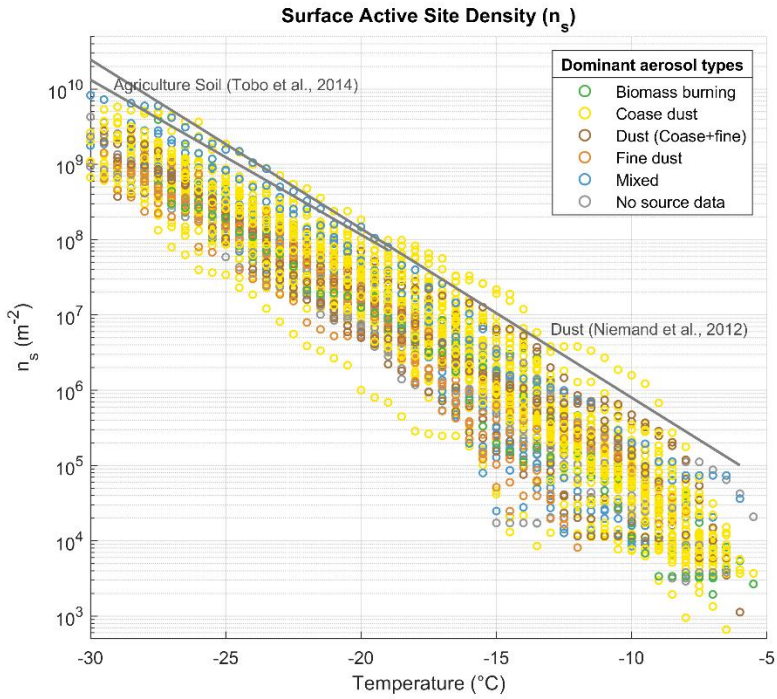

Figure S15. IN active surface site density (n_s, m^{-2}) calculated based on total surface area concentrations.

References:

Brey, S. J., Ruminski, M., Atwood, S. A., and Fischer, E. V.: Connecting smoke plumes to sources using Hazard Mapping System (HMS) smoke and fire location data over North America, Atmos. Chem. Phys., 18, 1745-1761, https://doi.org/10.5194/acp-18-1745-2018, 2018.

Guilbaud, C., Morris, C. E., Barakat, M., Ortet, P., and Berge, O.: Isolation and identification of Pseudomonas syringae facilitated by a PCR targeting the whole P. syringae group, FEMS Microbiol. Ecol., 92, fiv146, https://doi.org/10.1093/femsec/fiv146, 2016.

Niemand, M., Möhler, O., Vogel, B., Vogel, H., Hoose, C., Connolly, P., Klein, H., Bingemer, H., DeMott, P., Skrotzki, J., and Leisner, T.: A Particle-Surface-Area-Based Parameterization of Immersion Freezing on Desert Dust Particles, J. Atmos. Sci., 69, 3077-3092, https://doi.org/10.1175/Jas-D-11-0249.1, 2012.

Niño, L.: Nationwide Decadal Source Apportionment of $PM_{2.5}$ with a Focus on Iron, Colorado State University, 2021.

Tobo, Y., DeMott, P. J., Hill, T. C. J., Prenni, A. J., Swoboda-Colberg, N. G., Franc, G. D., and Kreidenweis, S. M.: Organic matter matters for ice nuclei of agricultural soil origin, Atmos. Chem. Phys., 14, 8521-8531, https://doi.org/10.5194/acp-14-8521-2014, 2014.